1-28-2020

Structural and biophysical analysis of the CLCA1 VWA domain suggests mode of TMEM16A engagement

Kayla N Berry

Tom J Brett

Article

Cell Reports

Structural and Biophysical Analysis of the CLCA1 VWA Domain Suggests Mode of TMEM16A Engagement

Graphical Abstract

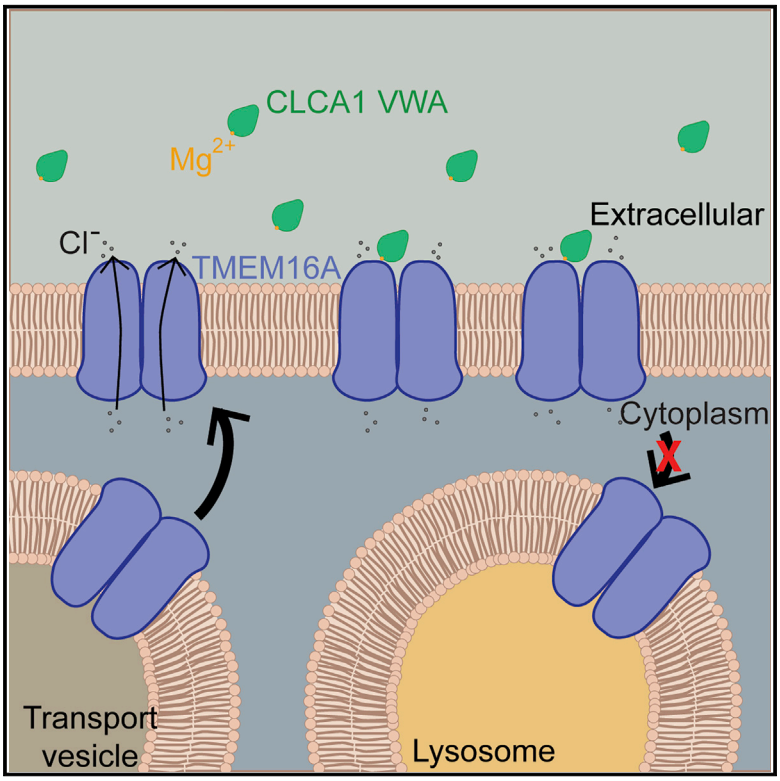

Authors

Kayla N. Berry, Tom J. Brett

Correspondence

tbrett@wustl.edu

In Brief

CLCA1 is a secreted potentiator of the calcium-activated chloride channel TMEM16A. Berry et al. report the structure and biophysical analysis of the human CLCA1 VWA domain, which binds to and potentiates TMEM16A. Their results suggest how the VWA MIDAS engages TMEM16A.

Highlights

- A 2.00-Å crystal structure of the CLCA1 VWA domain that potentiates TMEM16A is reported
- CLCA1 VWA MIDAS is in a high-affinity configuration with a disulfide bond nearby
- Crystal lattice pseudoligand contacts mimic engagement with TMEM16A

Berry & Brett, 2020, Cell Reports *30*, 1141–1151
January 28, 2020
https://doi.org/10.1016/j.celrep.2019.12.059

CellPress

Cell Reports
Article

Structural and Biophysical Analysis of the CLCA1 VWA Domain Suggests Mode of TMEM16A Engagement

Kayla N. Berry[1,2] and Tom J. Brett[2,3,4,5,6,*]
[1]Immunology Program and Medical Scientist Training Program, Washington University School of Medicine, St. Louis, MO 63110, USA
[2]Department of Internal Medicine, Division of Pulmonary and Critical Care, Washington University School of Medicine, St. Louis, MO 63110, USA
[3]Center for the Investigation of Membrane Excitability Diseases (CIMED), Washington University School of Medicine, St. Louis, MO 63110, USA
[4]Department of Cell Biology and Physiology, Washington University School of Medicine, St. Louis, MO 63110, USA
[5]Department of Biochemistry and Molecular Biophysics, Washington University School of Medicine, St. Louis, MO 63110, USA
[6]Lead Contact
*Correspondence: tbrett@wustl.edu
https://doi.org/10.1016/j.celrep.2019.12.059

SUMMARY

The secreted protein calcium-activated chloride channel regulator 1 (CLCA1) utilizes a von Willebrand factor type A (VWA) domain to bind to and potentiate the calcium-activated chloride channel TMEM16A. To gain insight into this unique potentiation mechanism, we determined the 2.0-Å crystal structure of human CLCA1 VWA bound to Ca^{2+}. The structure reveals the metal-ion-dependent adhesion site (MIDAS) in a high-affinity "open" conformation, engaging in crystal contacts that likely mimic how CLCA1 engages TMEM16A. The CLCA1 VWA contains a disulfide bond between α3 and α4 in close proximity to the MIDAS that is invariant in the CLCA family and unique in VWA structures. Further biophysical studies indicate that CLCA1 VWA is preferably stabilized by Mg^{2+} over Ca^{2+} and that α6 atypically extends from the VWA core. Finally, an analysis of TMEM16A structures suggests residues likely to mediate interaction with CLCA1 VWA.

INTRODUCTION

The calcium-activated chloride channel regulator 1 (CLCA1) is emerging as an important channel-modifying protein with poorly defined roles in health and disease (Patel et al., 2009; Sala-Rabanal et al., 2015a). CLCA1 is a secreted protein that binds to and potentiates the calcium-activated chloride channel TMEM16A (Sala-Rabanal et al., 2015b). In the airways and digestive tracts, anion channels play important roles in mediating mucus hydration and pH balance for protective and digestive purposes. CLCA1 and other CLCA family members have often been associated with airway and digestive manifestations. For example, animal models and clinical studies suggest a compensatory role for CLCAs in the context of cystic fibrosis (CF). The fatal intestinal disease meconium ileus that arises in cystic fibrosis transmembrane conductance regulator (CFTR)-deficient mice is corrected by overexpression of mouse CLCA1 (Young et al., 2007). Correspondingly, variants of either CLCA1 (van der Doef et al., 2010) or CLCA4 (Kolbe et al., 2013) have been linked to more severe meconium ileus in humans. In addition, the therapeutic peptide thymosin alpha 1 (Tα1) has been observed to rectify multiple airway and intestinal defects in a mouse model of CF, which may be partially due to increasing CLCA1 expression and, thus, potentiation of TMEM16A (Romani et al., 2017). By similar arguments, TMEM16A has emerged as a therapeutic target for CF and other muco-obstructive diseases (Li et al., 2017; Mall and Galietta, 2015; Sondo et al., 2014). Inhibiting microRNA (miRNA)-mediated knockdown of TMEM16A results in increased chloride flux and mucociliary clearance in CF cell lines, primary CF cells, and mouse models (Sonneville et al., 2017). Increased TMEM16A activity has also been linked to other processes that are important to the resolution of CF airway disease: cell migration and proliferation for wound healing (Ruffin et al., 2013; Sonneville et al., 2017) and suppression of inflammatory cytokine production (Veit et al., 2012). Based on these and other observations, both CLCA1 and TMEM16A have been suggested as targets for stimulation in muco-obstructive diseases—either to compensate or bypass dysfunctional CFTR in CF or to stimulate secretion to solubilize obstructive mucus in asthma and chronic obstructive pulmonary disease (COPD) (Mall et al., 2018). Such efforts require a detailed molecular level understanding of the mechanism of potentiation.

The ability of CLCA1 to potentiate TMEM16A is regulated by a matrix-metalloprotease-like (MMP-L) domain found in the N terminus of CLCA1. During secretion, CLCA1 MMP-L cleaves CLCA1 into two fragments, allowing the N-terminal fragment of CLCA1 (N-CLCA1) to engage TMEM16A (Yurtsever et al., 2012). This engagement is mediated between the von Willebrand factor type A (VWA) domain in CLCA1 and the α9-α10 loop in TMEM16A and increases the surface expression of TMEM16A, thereby increasing currents (Sala-Rabanal et al., 2015b, 2017). The CLCA1 VWA domain (CLCA1 VWA) alone is necessary and sufficient to potentiate TMEM16A (Sala-Rabanal et al., 2017). VWA domains commonly mediate protein-protein interactions, within which the integrin αI subfamily has been the most well-characterized structurally and biophysically (Luo et al., 2007). Most contain a

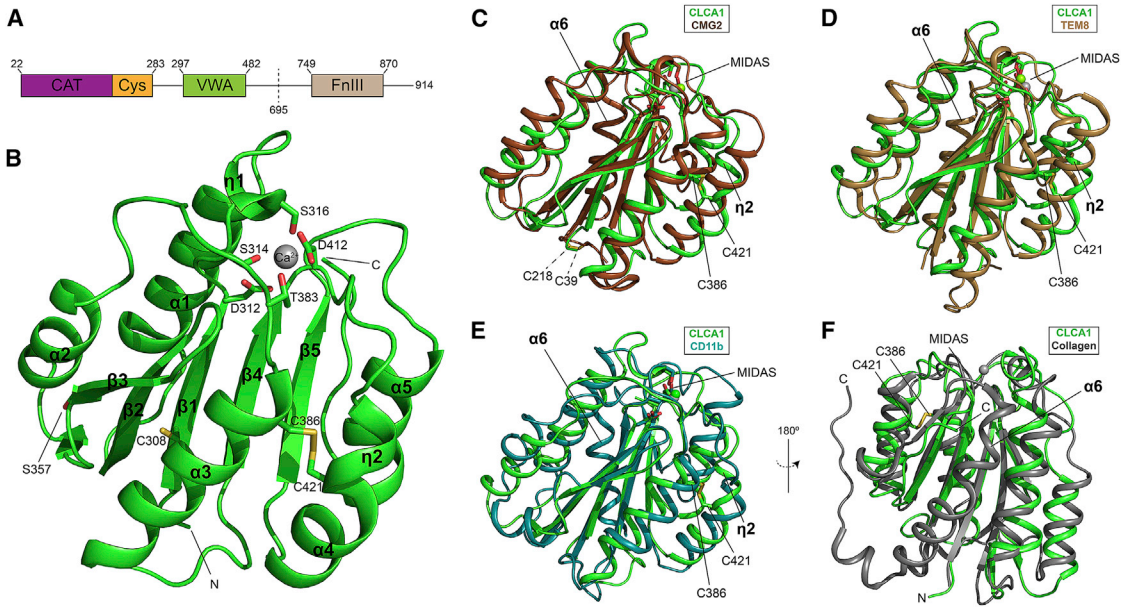

Figure 1. Structure of Human CLCA1 VWA Domain

(A) Domain architecture schematic of full-length human CLCA1. Labels denote the following domains: CAT, matrix-metalloprotease-like catalytic domain; Cys, matrix-metalloprotease-like cysteine-rich region; FnIII, fibronectin type III domain; VWA, von Willebrand factor type A. Numbers above the domains indicate approximate domain boundaries. Dashed line indicates cleavage site.

(B) Ribbon diagram of the human CLCA1 VWA domain structure obtained by X-ray crystallography. β strands and α and η helices of the VWA domain are labeled according to the vWFA2 nomenclature (Zhang et al., 2009). A calcium ion (Ca^{2+}) coordinated by the VWA MIDAS motif is shown as a gray sphere. MIDAS motif residues surrounding the divalent cation are highlighted. The three invariant cysteines and location of the disease-associated variant S357 are also labeled. N, N terminus; C, C terminus.

(C–F) Human CLCA1 VWA domain is superpositioned to anthrax toxin receptors CMG2 (PDB: 1SHU) (C) and TEM8 (PDB: 3N2N) (D), CD11b αI domain (PDB: 1IDO) (E), and collagen (PDB: 4IGI) (F) VWA domains. MIDAS motifs are indicated for all alignments. The η2 helix of the CLCA1 VWA domain and the α6 helices of the published VWA domain structures are labeled in (C)–(E). For all structures, the CLCA1 disulfide is annotated by solid lines. For (A), the natural disulfide in CMG2 is annotated by dashed lines. For (F), the N and C termini are labeled.

See also Figures S1 and S2.

metal-ion-dependent adhesion site (MIDAS) motif to mediate protein-protein interactions (Springer, 2006; Whittaker and Hynes, 2002). MIDAS motifs consist of a loop containing a DXSXS sequence, a second loop containing a threonine (T4), and a third loop containing an aspartate (D5) that acts to chelate and present a divalent cation (usually Mg^{2+}) to ligands containing acidic residues (Asp or Glu), which then complete the coordination sphere for the divalent cation upon binding (Luo et al., 2007). Sequence analysis indicates that these MIDAS residues are present in CLCA1 VWA (Whittaker and Hynes, 2002), and we have shown that this motif and the divalent cation are necessary for CLCA1 potentiation of TMEM16A (Sala-Rabanal et al., 2017).

VWA domains are found in a functionally diverse range of proteins, including blood coagulation factors (von Willebrand factor), complement factors (Springer, 2006), signaling receptors (α integrins; Shimaoka et al., 2002), toxin receptors (anthrax toxin receptors; Lacy et al., 2004a, 2004b; Santelli et al., 2004), extracellular matrix (collagen, Becker et al., 2014; and matrillin, Paulsson and Wagener, 2018), ion channel regulators or subunits (CLCAs, Patel et al., 2009; and $Ca_v1.1$ α2δ1, Dolphin, 2016), as well as in critical proteins in bacterial pathogens such as *Plasmodium* (Song et al., 2012) and *Toxoplasma* (Song and Springer, 2014). Structural and biophysical studies have been carried out for several of these proteins, with those from α integrins, von Willebrand factor, and complement factors being the best characterized (Springer, 2006). All adopt a Rossman fold composed of a β sheet surrounded by amphipathic α helices (Rossmann et al., 1974). However, there are often structural and functional features that are unique to distinct families of VWA domains (Becker et al., 2014; Song et al., 2012; Song and Springer, 2014; Springer, 2006). To date, no high-resolution structure has been determined for a VWA domain from the CLCA phylogenetic branch. All CLCA proteins, with the exception of the CLCA3 pseudogenes (Mundhenk et al., 2018), contain a central VWA domain (Figure 1). To gain insight into the unique structural features of CLCA VWA domains, as well as how CLCA1 VWA might engage TMEM16A, we determined the high-resolution crystal structure of CLCA1 VWA. The structural information suggests the mode by which CLCA1 engages TMEM16A and the most likely sites on TMEM16A where engagement occurs.

RESULTS

Crystal Structure of the CLCA1 VWA

Human CLCA1 VWA (Figure 1A) was purified from a mammalian cell expression system and was previously shown to be functional in potentiating TMEM16A when exogenously applied

Table 1. Crystallographic Statistics for Human CLCA1 VWA

Parameter	Data
Construct	302–476
Data collection statistics	
Space group	C2
Unit cell	
a, b, c (Å)	104.9, 71.8, 74.8
α, β, γ (°)	90, 109.8, 90
Source	ALS 4.2.2
Wavelength (Å)	1.0000
Resolution (Å)	58.05–2.00 (2.05–2.00)
R_{merge}	0.090 (1.814)
$CC_{1/2}$	0.998 (0.507)
Completeness (%)	98.3 (86.3)
Redundancy	6.4 (4.2)
I/σ (I)	10.7(0.6)
Refinement statistics	
R_{work} (%)	19.87
R_{free} (%)	22.51
Amino acid residues (#)	318
Waters (#)	148
RMSD bond length (Å)/angles (°)	0.011/1.181
Wilson B ($Å^2$)	36.7
Average B protein ($Å^2$)	44.57
Average B water ($Å^2$)	47.51
Average B Ca^{2+} ($Å^2$)	37.50
Ramachandran	
% Favored	96.82
% Allowed	3.18
% Outliers	0
Rotamer outliers (%)	3.53
Clashscore	3.41
Molprobity	1.74
Luzzati error	0.284
PDB ID	6PYO

Values shown in parantheses () represent the highest resolution shell. See also Table S2.

to HEK293 cells (Sala-Rabanal et al., 2017). The structure was determined by molecular replacement at a 2.0-Å resolution (Table 1). There are two molecules in the asymmetric unit (ASU) that are highly similar (Cα root-mean-square deviation [RMSD] of 0.3 Å; Figure S1). Therefore, unless otherwise noted, our analysis of CLCA1 VWA will refer to chain B. The general structural features are similar to other VWA domain folds: a core composed of 6 β strands sandwiched between α-helical bundles (Figure 1B). A DALI structure comparison revealed that the CLCA1 VWA shares the most three-dimensional similarity to anthrax toxin receptors CMG2 (Lacy et al., 2004b) and TEM8 (Fu et al., 2010) and to the voltage-dependent L-type calcium channel $Ca_v1.1$ subunit α2δ (Wu et al., 2015, 2016; Figures 1C–1E) with RMSDs ranging from 1.9–2.3 Å (Holm and Laakso, 2016). However, there are three notable exceptions in comparison to these VWA domains from other families. First, the β sheet core is usually encompassed by 6 α helices. Although the last α helix, α6 (using the nomenclature of the VWA2 domain; Zhang et al., 2009), is predicted by secondary structure predictions (JPRED4; Drozdetskiy et al., 2015; see Figure 3A) and is present in this construct (residues 302–476), we did not observe defined electron density for it. Also, a slightly longer construct (residues 302–478) did not yield a map with α6 clearly present (Figure S2; Table S2). The absence of α6 places the N and C termini of the CLCA1 VWA on opposite ends, much like the arrangement reported in the structure of a collagen VI VWA domain (Figure 1F; Becker et al., 2014). If in solution α6 is not packed against the domain (see Discussion), this could have implications for how the domains of CLCA1 are oriented relative to one another or may facilitate cleavage of the N-CLCA1 from C-CLCA1. Second, there is a disulfide bond in proximity of the MIDAS residues, linking α3 and η2 of α4 (Figure 1B). The cysteines in this disulfide linkage are unique to the CLCA family of VWA domains. Most VWA domains do not contain a disulfide bond, and if one is present, it usually connects the N- and C-terminal boundaries of the domain (Figure 1C). Third, there is a 3_{10} helix (η2) at the N terminus of α4 that ends with one of the disulfide-bonded cysteines (Figures 1B–1E). Beyond the secondary structure, CLCA1 VWA differs most in the loops surrounding the MIDAS, as would be expected, because these loops usually dictate ligand-binding specificities of VWA domains (Luo et al., 2007).

CLCA1 VWA Crystallizes with MIDAS in the Open Conformation

Most VWA domains mediate protein-protein interactions by a MIDAS motif, which partially coordinates a divalent cation in a manner that encourages completion of the coordination sphere by an acidic residue (Asp or Glu) contributed by the ligand (McCleverty and Liddington, 2003; Nolte et al., 1999; Shimaoka et al., 2003; Springer, 2006; Vorup-Jensen et al., 2003). MIDAS motifs have been observed to exist in two conformations that correspond to the affinity of the VWA domain for its ligand: an open, high-affinity configuration and a closed, low-affinity configuration (Shimaoka et al., 2003). The closed conformation is defined by MIDAS D5 serving as a direct chelator of the divalent cation, through which the motif partially satisfies its electrophilic nature (Figure 2D). In contrast, the open configuration is hallmarked by all the direct MIDAS chelators of the divalent cation being uncharged (threonine, serine, or waters), creating an electrophilic divalent cation whose coordination is best satisfied by an acidic residue contributed by the engaging ligand (Figure 2C). The human CLCA1 VWA contains a perfectly conserved MIDAS motif (Whittaker and Hynes, 2002): a DXSXS sequence followed several residues later by a threonine (T383) and a final aspartate (D412) (Figure 2A). Strong density corresponding to an ion was observed at the center of this site for both molecules in the ASU (Figure S3). As the CLCA1 VWA was crystallized in conditions containing high $CaCl_2$ concentrations, we modeled a Ca^{2+} into the MIDAS site. Very few VWA domains have been crystallized in the presence of Ca^{2+} and instead usually contain Mg^{2+} or Mn^{2+} that bind at a higher affinity. Most VWA MIDAS motifs favor occupancy by Mg^{2+} rather than

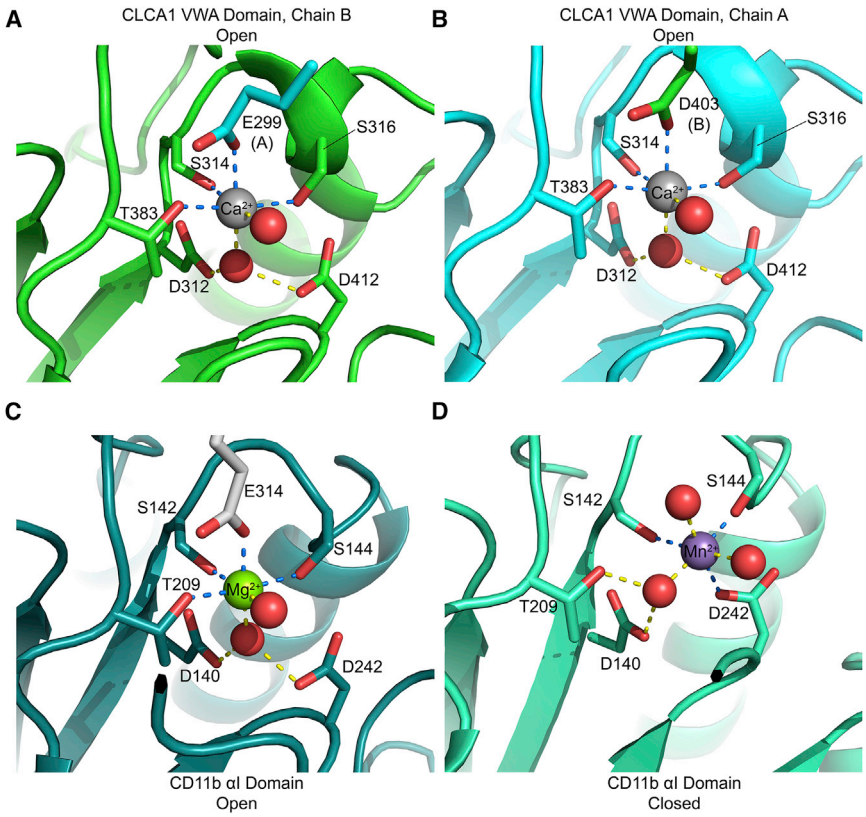

Figure 2. CLCA1 VWA MIDAS Crystallizes in an Open Conformation

(A–D) MIDAS regions of human CLCA1 chain B (A, in green) and chain A (B, in cyan) of the asymmetric unit and of the open (C) and closed (D) MIDAS configurations of the CD11b αI domain (PDB: 1IDO and 1JLM, respectively).

For (A)–(C), the pseudoligand residue is shown in the color of the appropriate chain. Waters are depicted as red spheres. Bonds coordinating divalent cations are shown as blue dashes (for direct side chain interactions) and yellow dashes (for indirect or water-mediated interactions).

See also Figure S3.

Ca^{2+}, and Mg^{2+} coordination usually results in higher-affinity binding to ligand or greater functional capability (Ajroud et al., 2004; Baldwin et al., 1998; San Sebastian et al., 2006; Vorup-Jensen et al., 2007). However, attempts to obtain CLCA1 VWA crystals in the presence of excess $MgCl_2$ were not successful.

For both molecules in the ASU, the structure reveals the MIDAS in the open, high-affinity conformation, with S314, S316, and T383 directly coordinating a calcium ion and D312 and D412 indirectly coordinating through a water molecule (Figures 2A and 2B). This coordinating geometry is consistent with our functional studies that showed (1) mutation of MIDAS residues, particularly T383 and S316, which both directly coordinate the divalent cation in the open conformation; and (2) chelation of extracellular Mg^{2+} by EDTA abrogated CLCA1 VWA-mediated potentiation of TMEM16A in whole-cell patch clamp experiments (Sala-Rabanal et al., 2017). An acidic residue from an adjacent molecule in the crystal, either a glutamate from chain A (E299) or aspartate (D403) from chain B, completes the coordination of the calcium ion. This arrangement is identical to the open conformation observed for the CD11b αI domain (Figure 2C) with the exception that, unlike the CD11b structure reported by Mahalingam et al. (Mahalingam et al., 2011), the acidic residue appears to mediate a monodentate interaction with calcium rather than a bidentate interaction. Such crystal contact "pseudoligand" interactions are commonly observed in crystal structures of VWA domains that utilize their MIDAS motif to mediate interactions (Bhattacharya et al., 2004; Lacy et al., 2004b; Lee et al., 1995; Li et al., 1998). The presence of the open conformation in our structures implies that the CLCA1 VWA likely adopts this configuration for a high-affinity interaction with TMEM16A and also suggests that the binding is primarily mediated by a critical acidic residue within TMEM16A.

An Invariant Disulfide Bond Is Required for Folding and Secretion of CLCA1 VWA

Our high-resolution crystal structure of CLCA1 VWA revealed a disulfide bond between C386 and C421, connecting α3 and the η2 segment of α4 (Figure 1B). This disulfide bond is unique in that (1) natural disulfide bonds in VWA domains are not common; and (2) unlike CMG2 (Lacy et al., 2004b), MIC2 (Song et al., 2012) and TRAP (Song and Springer, 2014), VWA domains in which a disulfide bond is found linking the N- and C-termini, the disulfide bridge in the CLCA1 VWA is found in close proximity to the MIDAS. Interestingly, sequence analysis indicates that CLCA proteins have three invariant cysteines within the VWA domain (Figure 3A; Patel et al., 2009). The free cysteine C308 is packed within the core of CLCA1 VWA (0% sidechain solvent accessibility as calculated by NACCESS; Hubbard and Thornton, 1993; Figure 1B). This likely negates the possibility that CLCA1 VWA may covalently bind to itself or to other proteins, as is the case for some VWA domains, such as the Ca_v-1 and −2 calcium channel α2 subunits, which remain covalently linked to the δ subunit by a disulfide bond (Wu et al., 2015, 2016) after proteolytic cleavage. To investigate the structural importance of invariant cysteines in the CLCA1 VWA, we carried out mutations to serine (C308S, C386S, C421S, and C386S/C421S) and expressed them in HEK293T cells. Although all proteins were expressed, only the C308S mutant was secreted (Figure 3B), indicating that mutants with disrupted disulfide bond formation were misfolded and retained in the secretory pathway. Further supporting this observation, for the mutants that were not secreted, a band at approximately twice the monomer size of CLCA1 VWA (2 X 20kDa) was observed in cell lysates, suggesting that aberrant disulfide bonds between molecules may have been formed during misfolding and not sufficiently reduced in SDS-PAGE (Figure 3B). To assess the role of this disulfide in CLCA1 VWA stability, we carried out circular dichroism (CD) and

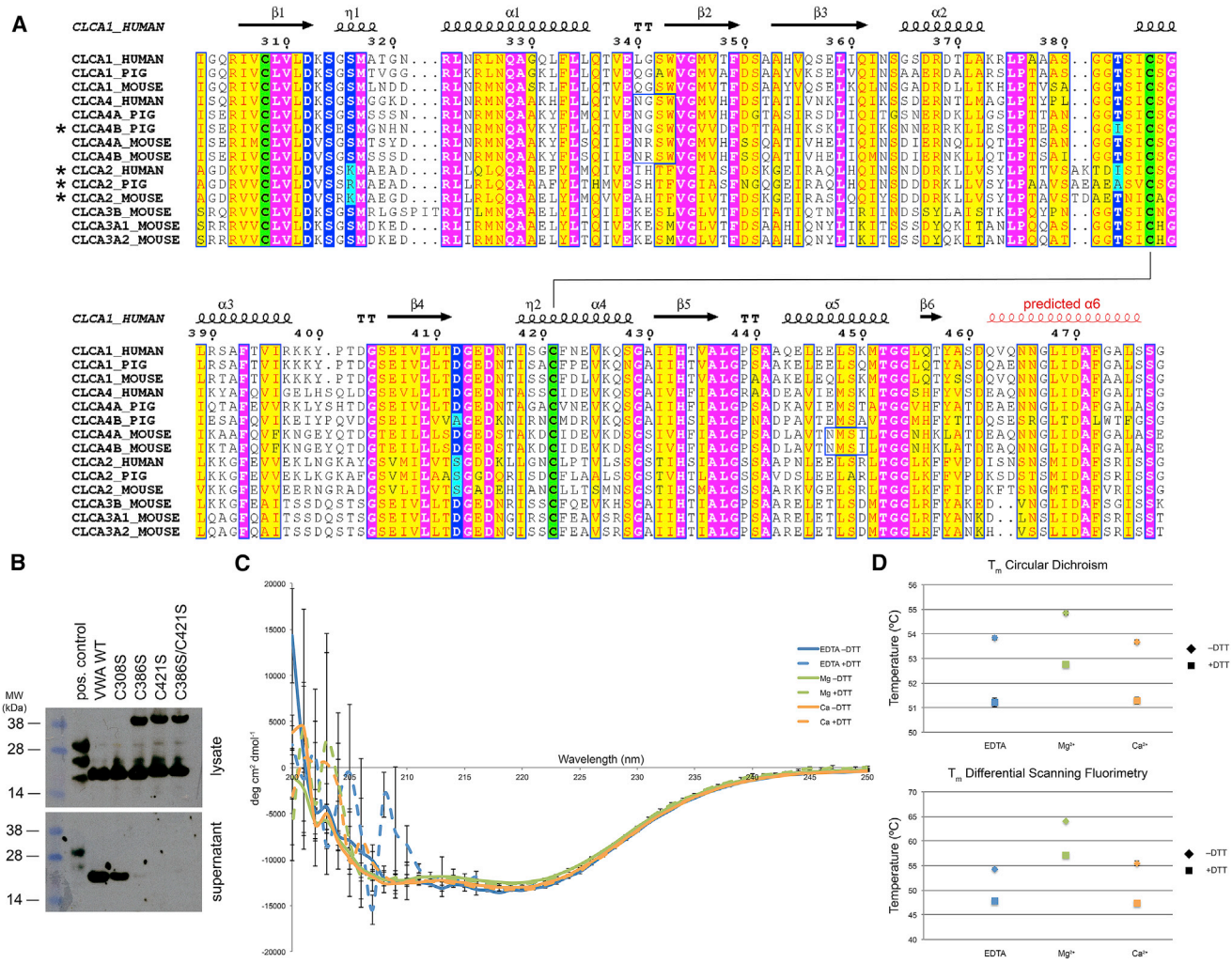

Figure 3. Biophysical Analysis of CLCA Family VWA Domain Invariant Cysteines

(A) Annotated sequence alignment for human, mouse, and pig CLCA VWA domains. Numbering corresponds to the sequence of human CLCA1. Secondary structure of human CLCA1 is labeled above. A solid line indicates the disulfide bond observed in the crystal structure. Stars next to the sequence indicate that the VWA domain contains an imperfect MIDAS (Whittaker and Hynes, 2002). Sequences are shown for hCLCA1 (GenBank: NM_001285.3), pCLCA1 (NM_214148.1), mCLCA1 (NM_017474.2), hCLCA4 (NM_012128.3), pCLCA4a (XM_001926978.5), pCLCA4b (XM_003125934.5), mCLCA4a (NM_207208), mCLCA4b (NM_001033199), hCLCA2 (NM_006536.6), pCLCA2 (XM_003125930.4), mCLCA2 (NM_178697.5), mCLCA3b (NM_139148), mCLCA3a1 (NM_009899), and mCLCA3a2 (NM_030601) (where h, human; p, pig; m, mouse). Sequence conservation is color coded as follows: invariant residues (with the exception of cysteine and invariant MIDAS residues), magenta; invariant cysteines, green; residues with a global similarity score of 0.75 or higher as determined by ESPript 3.0 software (Robert and Gouet, 2014a), yellow; perfect MIDAS residues, blue; and imperfect MIDAS residues, cyan. Black boxes indicate the most strongly predicted sites of N-linked glycosylation by NetNGlyc 1.0 software (Blom et al., 2004). The predicted α6 helix (JPRED4; Drozdetskiy et al., 2015) of the CLCA1 VWA domain is labeled above the alignment in red. MIDAS residues are highlighted in purple. Invariant cysteines are labeled in yellow.

(B) Wild-type (WT) CLCA1 VWA domain and cysteine-to-serine mutants of the invariant disulfides (single mutants C308S, C386S, and C421S, and double mutant C386S/C421S) were expressed in 293T cells. Supernatants and lysates were analyzed by western blot (anti-6-His). Pos. control, 6-histidine tagged MAM domain from receptor tyrosine phosphatase μ (SDS-PAGE molecular weight [MW] = 30 kDa).

(C) Circular dichroism spectra of the human CLCA1 VWA domain in the presence of EDTA (blue), magnesium (green), and calcium (orange), with (dashed line) or without (solid line) reducing agent (DTT). Spectra are plotted as mean ellipticity per residue ± SD of triplicate recordings. Representative spectra of three independent experiments.

(D) Thermal denaturation of human CLCA1 VWA domain by determination of melting temperatures (T_M) by monitoring circular dichroism at 222 nm (top panel) or differential scanning fluorimetry (bottom panel) in the presence of EDTA (blue), magnesium (green), and calcium (orange), with (squares) and without (diamonds) reducing agent (DTT). Representative T_Ms of three independent experiments. For circular dichroism, data are represented as the calculated T_M and estimated error from the ProScan software. For differential scanning fluorimetry, data are represented as mean ± SEM of triplicate samples.

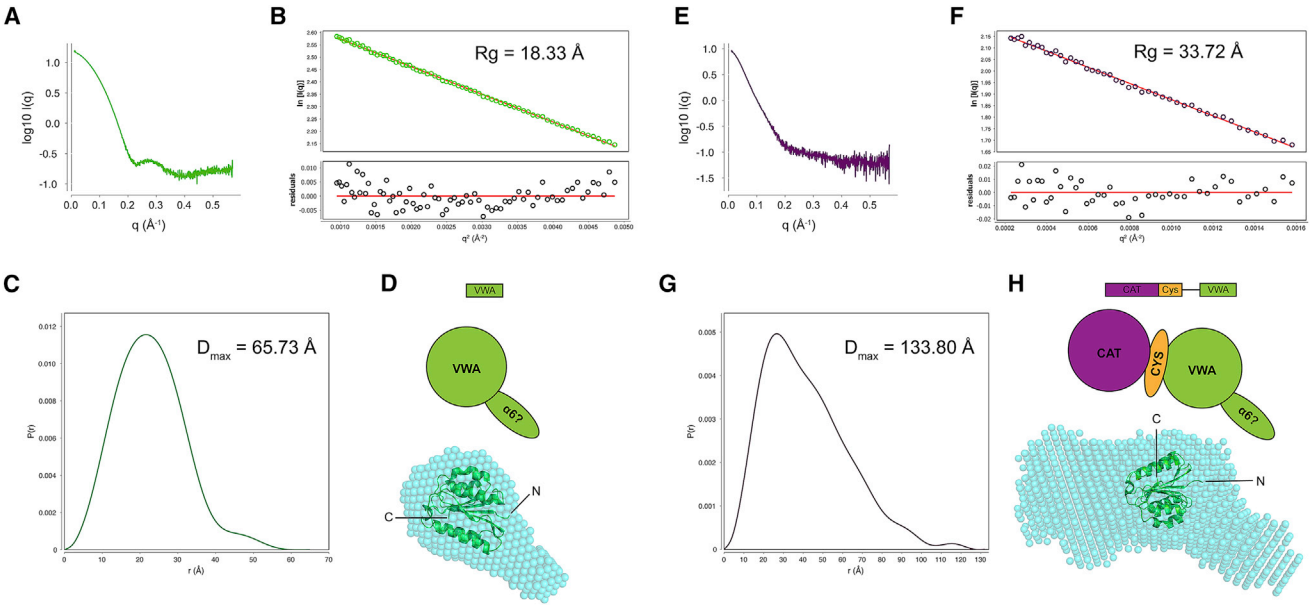

Figure 4. Solution Structures of CLCA1 VWA and CAT-CYS-VWA Proteins from SAXS Analysis

Solution SAXS for human CLCA1 VWA (302–476) (A–D) and CLCA1 E157Q (22–477) encompassing the MMP-L catalytic domain (CAT), cysteine-rich region (Cys), and VWA (E–H).

(A and E) Raw SAXS data.

(B and F) Top panel, Guinier regions with SAXS data points (open circles) and fits (solid red line). Radius of gyration (R_g) is labeled above the line of fit. Bottom panel, residual data points (open circles) of Guinier region with fits (solid red line).

(C and G) Distance distribution functions. D_{max} is indicated next to the distribution.

(D and H) *Ab initio* SAXS envelope models. Models are the average of 10 independent DAMMIN predictions averaged in DAMAVER. CLCA1 VWA domain was docked into the envelope using SITUS. Domain architecture schematics and cartoons are labeled above the SAXS envelopes. in (D) and (H). N and C termini are labeled.

differential scanning fluorimetry (DSF) experiments. CD spectra of CLCA1 VWA in the absence of divalent cations (+EDTA) varied greatly with the addition of DTT, especially at wavelengths of <215 nm, indicating partial unfolding upon reduction of the disulfide bond (Figure 3C). In addition, thermal denaturation studies by CD and DSF in the presence or absence of DTT showed that reduction of the disulfide bond decreased the melting temperature (T_M) by 2.6°C and 6.5°C, respectively (Figure 3D). Altogether, these results suggest that CLCA family VWA domains contain an invariant disulfide that is required for folding and stability. The role of the invariant free cysteine (C308) is unclear at this time. However, it should be noted that the sidechain sulfhydryl does hydrogen bond to the backbone carbonyl of L309, so this sidechain likely contributes to the stability of the fold.

CLCA1 VWA Is Stabilized by 1 mM Mg^{2+} but Not Ca^{2+}

Our crystallization studies seemed to indicate that CLCA1 VWA might not preferentially bind Mg^{2+}, as we were unable to obtain crystals in the presence of Mg^{2+}. This would be unusual because VWA domains normally bind Mg^{2+} with affinities in the low micromolar range, with affinities for Ca^{2+} about 100-fold worse, in the range of hundreds of micromolar (Ajroud et al., 2004; Baldwin et al., 1998; San Sebastian et al., 2006; Vorup-Jensen et al., 2007). To relatively rank the binding affinities of CLCA1 VWA for the divalent cations, we assessed whether Ca^{2+} or Mg^{2+} impacted thermal stability by using CD and DSF thermal denaturation experiments. Both analyses were consistent: Mg^{2+} significantly stabilizes the VWA domain over Ca^{2+} or cation-free conditions (+EDTA), increasing the T_M of CLCA1 VWA by 1.0°C–1.2°C by CD and 8.6°C–9.8°C by DSF (Figure 3D). In addition, Mg^{2+} even stabilized CLCA1 VWA under reducing conditions (ΔT_M = +2.1°C or +6.9°C, by CD and DSF, respectively). In contrast, the addition of 1 mM Ca^{2+} was unable to shift the T_M of CLCA1 VWA compared to cation-free conditions. These results are consistent with previous investigations of VWA domain affinities for divalent cations (Ajroud et al., 2004; Baldwin et al., 1998; San Sebastian et al., 2006; Vorup-Jensen et al., 2007) and indicate that CLCA1 VWA preferentially binds Mg^{2+} over Ca^{2+}.

Solution Structures of CLCA1 Suggest VWA α6 Extends from the Core Fold

Because we were unable to observe definitive electron density for the CLCA1 VWA α6 in our high-resolution crystal structure, we utilized small-angle X-ray scattering (SAXS) to develop a low-resolution envelope structure of the VWA domain (Figures 4A–4D) as well as CLCA1 containing the catalytic and VWA domains with an inactivating mutation in the MMP-L domain (CAT-CYS-VWA E157Q) (Figures 4E–4H). The CLCA1 VWA structure was docked into these envelopes using SITUS. Both envelopes display globular regions consistent with one-domain (VWA; Figure 4D) or three-domain (CAT-CYS-VWA E157Q; Figure 4H) proteins. However, both also included a

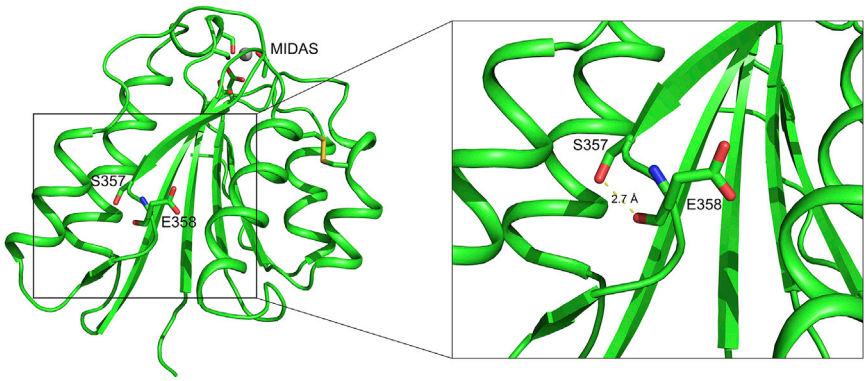

Figure 5. Disease-Associated Residue S357 Sidechain Engages in an Intramolecular Hydrogen Bond

The sidechain of S357 and the backbone and sidechain of E358 are highlighted. The sidechain hydroxyl of S357 forms a hydrogen bond to the backbone carbonyl of E358 (indicated by the dashed yellow line).

tubular tail extending from the sphere in both envelopes. In light of the missing α6 helix in our crystal structure, we speculate that this tail may represent the α6 helix that cannot be resolved in the crystal structure because it does not pack tightly against the rest of the domain. Analysis of packing in the CLCA1 VWA crystal shows that the C terminus for the built structure is located adjacent to large solvent channels that would allow for multiple positions for an α6 helix that extends from the core VWA. Thus, solution structural studies by SAXS suggest that CLCA1 VWA α6 extends from the VWA core fold, in contrast to other structurally characterized VWA domains.

Structural Insights into the Disease-Associated CLCA1 Variant S357N

In genomic analyses, S357N has been identified as a mutation modifying the severity of intestinal disease occurring in CF patients, as it was associated with aggravated meconium ileus (van der Doef et al., 2010). To gain mechanistic insight into how this mutation might manifest in disease, we analyzed the structural environment of S357 in our CLCA1 VWA structure. S357 is found distal to the MIDAS motif, and the sidechain hydroxyl donates a hydrogen bond to the backbone carbonyl of the adjacent residue (E358) (Figure 5). This results in the S357 sidechain being mostly buried (4.8% side chain solvent accessibility by NACCESS). Given the tightly packed environment, it is highly unlikely that an asparagine at this position would be able to engage in the same hydrogen bond, which might disrupt folding or folding kinetics and could result in reduced expression levels. This would result in decreased potentiation of calcium-activated chloride currents, reducing hydration and resulting in thick mucus plugging of the intestine. This would be consistent with our published functional studies in overexpression systems in which S357N does not affect the ability of CLCA1 VWA to potentiate chloride currents by TMEM16A (Sala-Rabanal et al., 2017). This is also consistent with studies in CFTR knockout mice that show that mouse CLCA1 expression is decreased in mice with aggravated meconium ileus, which is rescued by overexpression of mouse CLCA1 (Young et al., 2007).

Structural Implications for CLCA1 VWA Engagement of TMEM16A

Our crystal structure of CLCA1 VWA reveals the MIDAS in the high-affinity open configuration and engaging in pseudoligand interactions with crystal lattice neighbors. These interactions mimic the mode by which CLCA1 VWA would engage TMEM16A. In our previous studies, we showed that an antibody targeting the TMEM16A α9-α10 loop could block binding of CLCA1 (Sala-Rabanal et al., 2015b). This result, in combination with our current structural observations, suggests that an acidic residue located in the TMEM16A α9-α10 loop is primarily responsible for mediating interaction with the CLCA1 VWA MIDAS. To identify the most likely candidate residues, we analyzed the recently determined cryoelectron microscopy (cryo-EM) structures of mouse TMEM16A (Dang et al., 2017; Paulino et al., 2017), making note of which acidic residues in this loop were most solvent exposed. This loop contains 9 acidic residues, 5 of which are highly solvent exposed (>60% sidechain solvent-accessible surface in NACCESS) (Figure 6). These residues are all conserved in human TMEM16A (corresponding to D851, D854, E858, E869, and E874). Thus, one of these five residues is most likely responsible for mediating the interaction with CLCA1. Similar modes of engagement have been observed in the voltage-gated calcium channels system, such as $Ca_v1.1$, where cryo-EM structures reveal an interaction with the α2δ subunit VWA that appear to be primarily mediated by a single acidic residue in the channel domain (Wu et al., 2015, 2016). However, it is worth noting that more complex models, such as three-way modes of engagement, have also been suggested in this system (Briot et al., 2018). Future mutational, functional, and structural studies will be required to identify which residues in TMEM16A are responsible.

DISCUSSION

Here, we present the structural and biophysical analysis of the CLCA1 VWA, the first structural characterization of a VWA domain from the CLCA family of channel-modifying proteins. Our analysis reveals major observations with respect to CLCA function and a potential role in disease. First, our structure reveals the MIDAS motif in the high-affinity open conformation, engaging in pseudoligand contacts that mimic the mode by which it would engage TMEM16A and suggesting that one of five acidic residues in the α9-α10 loop are primarily responsible for mediating the interaction (Figure 6). However, it should be noted that the other two extracelluar loops in TMEM16A (α1-α2 loop and α5-α6 loop) in the cryo-EM structure are in close proximity to the α9-α10 loop (Paulino et al., 2017), and therefore, antibody binding to the α9-α10 loop could potentially sterically hinder access to these loops as well. So, potential involvement of these

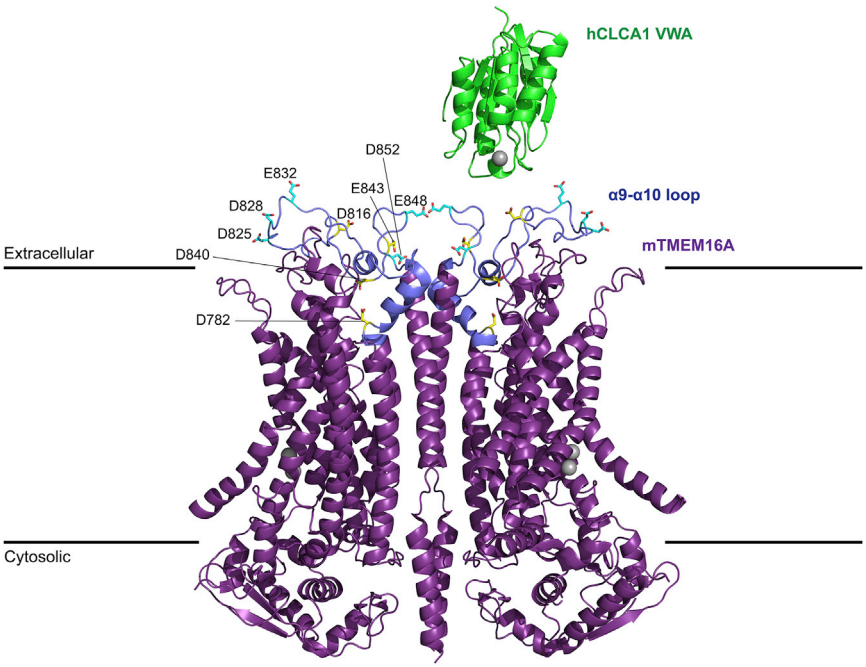

Figure 6. Most Probable Sites of CLCA1-TMEM16A Interaction Suggested by Structural and Functional Studies

The cryo-EM model of mouse TMEM16A (mTMEM16A) dimer (PDB: 5OYB; Paulino et al., 2017) (purple) with the α9-α10 loop (blue) and labeled acidic residues in this loop shown in either yellow (<60% solvent-accessible surface for sidechain) or cyan (>60% solvent-accessible surface for sidechain). CLCA1 VWA (green) is poised on the extracellular face of mTMEM16A, as our structural data suggest that interaction with CLCA1 VWA MIDAS is likely mediated by one of these residues. Divalent cations (Ca^{2+}) are shown in gray.

loops in engagement should not be ruled out. Analysis of sequence alignments across species indicate that most CLCA4 proteins contain an intact MIDAS motif, whereas most CLCA2 family members do not, missing one or two key residues (Figure 3A). Because members of the CLCA2 family have been observed to potentiate calcium-dependent chloride currents (Gruber et al., 1999), this would indicate that either neighboring residues compensate to complete a non-standard MIDAS motif or CLCA2 proteins carry out this function utilizing a different mode of engagement. Our crystal and solution structures suggest that α6 of the CLCA1 VWA extends from the core, which may potentially contribute to the CLCA1 VWA MIDAS being accessible to engage TMEM16A by directing trailing domains further away from the VWA core structure.

CLCA VWA domains contain three cysteines that are invariant across species (Figure 3A). Two of them (corresponding to C386 and C421 in CLCA1) engage in a disulfide bond that is unique compared to other structurally characterized VWA domains. This linkage appears to be required for folding and stability of the domain. In addition, this disulfide is in close proximity to key residues of the MIDAS motif. This disulfide bond appears to bend the η2 helix toward the MIDAS and possibly constrain both the α2-α3 and the β4- η2 loops, which contain the conserved MIDAS threonine (T383) and aspartic acid (D412), respectively, potentially favoring the open configuration (Figures 2A–2C). It is interesting to note that in the shift from an open to a closed MIDAS configuration, it is these two MIDAS residues that alter their coordination to the divalent cation (i.e., in the open configuration, threonine directly coordinates the cation and the second aspartic acid indirectly coordinates through water, but in a closed configuration, threonine indirectly coordinates by water and the second aspartic acid directly coordinates the cation) (Figures 2C and 2D; Shimaoka et al., 2003). This disulfide, however, does not appear to shift the MIDAS preference for binding divalent cations. Previous computational and biophysical studies on αI domains indicate that Mg^{2+} is preferred to Ca^{2+} by 100- to 1,000-fold affinity (Ajroud et al., 2004; Baldwin et al., 1998; San Sebastian et al., 2006; Vorup-Jensen et al., 2007). Our thermal denaturation studies suggest similar trends for the CLCA1 VWA, indicating that at near physiological concentrations (1 mM), Mg^{2+} is preferred over Ca^{2+} and is likely the cation that mediates the CLCA1-TMEM16A interaction *in vivo*. The third invariant cysteine (C308 in CLCA1) is not required for folding or stability. Interestingly, the *Toxoplasma gondii* motility and invasion protein MIC2 also has a cysteine in this position of β1 that, in contrast, engages in a disulfide linkage with α4 (C164) in its VWA domain (Song and Springer, 2014). This is not the case in CLCA VWAs, as the structurally corresponding position (A392 located in α3 of CLCA1) is either an alanine or glycine (Figure 3A). It is unclear at this time what its functional role is and why it is invariant at this position.

The S357N variant of CLCA1 has been associated with increased severity of meconium ileus in CF patients (van der Doef et al., 2010). This residue is tightly packed and engages in a stabilizing hydrogen bond with the backbone. It is unlikely that a mutation to asparagine would be well accommodated at this position. Thus, this mutation likely impacts the expression level of CLCA1, thereby decreasing the ability to potentiate TMEM16A. Clinical and animal model studies further support the concept that reduced CLCA1 and TMEM16A activity contributes to pathology in the CF airway and intestinal diseases. For example, miRNA targeting TMEM16A is overexpressed in CF airways, and inhibiting this miRNA-mediated knockdown of TMEM16A results in increased chloride flux and mucociliary clearance by TMEM16A in CF cell lines, primary CF cells, and mouse models (Sonneville et al., 2017). In addition, the peptide drug thymosin alpha 1 (Tα1) has been demonstrated to increase anion conductance in F508del-CFTR airway cell lines and mice, and depleting CLCA1 with small interfering RNA (siRNA) greatly reduces the ion channel activity enhanced by Tα1 (Benedetto et al., 2017). Furthermore, CFTR-deficient mice with increased meconium ileus display lower CLCA1 expression

that is corrected by the overexpression of CLCA1 (Young et al., 2007). Altogether, these published observations and our previous results suggest that CLCA1-mediated enhancement of TMEM16A activity plays an important role in mucosal inflammatory diseases and, thereby, represents a viable therapeutic target. Our structural results and analysis provide an important framework for studying the role of CLCA proteins in health and disease.

STAR★METHODS

Detailed methods are provided in the online version of this paper and include the following:

- KEY RESOURCES TABLE
- LEAD CONTACT AND MATERIALS AVAILABILITY
- EXPERIMENTAL MODEL AND SUBJECT DETAILS
  - Cell Lines
- METHOD DETAILS
  - Expression constructs
  - Protein expression and purification
  - Crystallization, structure determination, and analysis
  - Small angle X-ray scattering
  - Heterologous expression of CLCA1 and Western Blotting
  - Circular Dichroism
  - Differential Scanning Fluorimetry
- QUANTIFICATION AND STATISTICAL ANALYSIS
- DATA AND CODE AVAILABILITY

SUPPLEMENTAL INFORMATION

Supplemental Information can be found online at https://doi.org/10.1016/j.celrep.2019.12.059.

ACKNOWLEDGMENTS

This work was supported by NIH R01-HL119813 (to T.J.B.), NIH UL1TR002345 (pilot to T.J.B.), CIMED Pilot and Feasibility Grant (to T.J.B.), Cystic Fibrosis Foundation BRETT-G018 (to T.J.B.), NIH F30-HL140783 (to K.N.B.), NIH T32-HL007317 (to K.N.B.), and T32-GM007200 (to K.N.B.). Results were derived from work performed at the Advanced Light Source, Berkeley, CA (ALS), beamline 4.2.2 (The Molecular Biology Consortium), and the SYBILS HT-SAX beamline 12.3.1. ALS is supported by the Office of Basic Energy Sciences of the U.S. DOE (DE-AC02-05CH11231), the Integrated Diffraction Analysis Technologies (IDAT) program, and supported by DOE Office of Biological and Environmental Research. Additional support comes from the NIH project ALS-ENABLE (P30 GM124169) and a High-End Instrumentation Grant, S10OD018483. We thank Prof. Greg R. Bowman for use of the Chirascan CD spectrophotomer and Catherine R. Knoverek for technical assistance with CD experiments.

AUTHOR CONTRIBUTIONS

K.N.B. executed experiments. K.N.B. and T.J.B. planned experiments, analyzed results, and wrote the manuscript.

DECLARATION OF INTERESTS

The authors declare no conflicts of interest.

Received: September 4, 2019
Revised: November 14, 2019
Accepted: December 16, 2019
Published: January 28, 2020

REFERENCES

Adams, P.D., Afonine, P.V., Bunkóczi, G., Chen, V.B., Davis, I.W., Echols, N., Headd, J.J., Hung, L.-W., Kapral, G.J., Grosse-Kunstleve, R.W., et al. (2010). PHENIX: a comprehensive Python-based system for macromolecular structure solution. Acta Crystallogr. D Biol. Crystallogr. *66*, 213–221.

Ajroud, K., Sugimori, T., Goldmann, W.H., Fathallah, D.M., Xiong, J.P., and Arnaout, M.A. (2004). Binding Affinity of Metal Ions to the CD11b A-domain Is Regulated by Integrin Activation and Ligands. J. Biol. Chem. *279*, 25483–25488.

Aricescu, A.R., Lu, W., and Jones, E.Y. (2006). A time- and cost-efficient system for high-level protein production in mammalian cells. Acta Crystallogr. D Biol. Crystallogr. *62*, 1243–1250.

Baldwin, E.T., Sarver, R.W., Bryant, G.L., Jr., Curry, K.A., Fairbanks, M.B., Finzel, B.C., Garlick, R.L., Heinrikson, R.L., Horton, N.C., Kelley, L.L., et al. (1998). Cation binding to the integrin CD11b I domain and activation model assessment. Structure *6*, 923–935.

Becker, A.K., Mikolajek, H., Paulsson, M., Wagener, R., and Werner, J.M. (2014). A structure of a collagen VI VWA domain displays N and C termini at opposite sides of the protein. Structure *22*, 199–208.

Benedetto, R., Ousingsawat, J., Wanitchakool, P., Zhang, Y., Holtzman, M.J., Amaral, M., Rock, J.R., Schreiber, R., and Kunzelmann, K. (2017). Epithelial Chloride Transport by CFTR Requires TMEM16A. Sci. Rep. *7*, 12397.

Bhattacharya, A.A., Lupher, M.L., Jr., Staunton, D.E., and Liddington, R.C. (2004). Crystal structure of the A domain from complement factor B reveals an integrin-like open conformation. Structure *12*, 371–378.

Blom, N., Sicheritz-Pontén, T., Gupta, R., Gammeltoft, S., and Brunak, S. (2004). Prediction of post-translational glycosylation and phosphorylation of proteins from the amino acid sequence. Proteomics *4*, 1633–1649.

Briot, J., Mailhot, O., Bourdin, B., Tétreault, M.P., Najmanovich, R., and Parent, L. (2018). A three-way inter-molecular network accounts for the $Ca_V\alpha2\delta1$-induced functional modulation of the pore-forming $Ca_V1.2$ subunit. J. Biol. Chem. *293*, 7176–7188.

Dang, S., Feng, S., Tien, J., Peters, C.J., Bulkley, D., Lolicato, M., Zhao, J., Zuberbühler, K., Ye, W., Qi, L., et al. (2017). Cryo-EM structures of the TMEM16A calcium-activated chloride channel. Nature *552*, 426–429.

Dolphin, A.C. (2016). Voltage-gated calcium channels and their auxiliary subunits: physiology and pathophysiology and pharmacology. J. Physiol. *594*, 5369–5390.

Drozdetskiy, A., Cole, C., Procter, J., and Barton, G.J. (2015). JPred4: a protein secondary structure prediction server. Nucleic Acids Res. *43*, W389–W394.

Dyer, K.N., Hammel, M., Rambo, R.P., Tsutakawa, S.E., Rodic, I., Classen, S., Tainer, J.A., and Hura, G.L. (2014). High-throughput SAXS for the characterization of biomolecules in solution: a practical approach. Methods Mol. Biol. *1091*, 245–258.

Emsley, P., Lohkamp, B., Scott, W.G., and Cowtan, K. (2010). Features and development of Coot. Acta Crystallogr. D Biol. Crystallogr. *66*, 486–501.

Franke, D., and Svergun, D.I. (2009). *DAMMIF*, a program for rapid *ab-initio* shape determination in small-angle scattering. J. Appl. Cryst. *42*, 342–346.

Franke, D., Petoukhov, M.V., Konarev, P.V., Panjkovich, A., Tuukkanen, A., Mertens, H.D.T., Kikhney, A.G., Hajizadeh, N.R., Franklin, J.M., Jeffries, C.M., and Svergun, D.I. (2017). *ATSAS 2.8*: a comprehensive data analysis suite for small-angle scattering from macromolecular solutions. J. Appl. Cryst. *50*, 1212–1225.

Fu, S., Tong, X., Cai, C., Zhao, Y., Wu, Y., Li, Y., Xu, J., Zhang, X.C., Xu, L., Chen, W., and Rao, Z. (2010). The structure of tumor endothelial marker 8 (TEM8) extracellular domain and implications for its receptor function for recognizing anthrax toxin. PLoS One *5*, e11203.

Gruber, A.D., Schreur, K.D., Ji, H.L., Fuller, C.M., and Pauli, B.U. (1999). Molecular cloning and transmembrane structure of hCLCA2 from human lung, trachea, and mammary gland. Am. J. Physiol. *276*, C1261–C1270.

Holm, L., and Laakso, L.M. (2016). Dali server update. Nucleic Acids Res. *44*, W351–W355.

Hubbard, S., and Thornton, J. (1993). NACCESS, Computer Program (Department of Biochemistry and Molecular Biology, University College London).

Kabsch, W. (2010). Xds. Acta Crystallogr. D Biol. Crystallogr. *66*, 125–132.

Kober, D.L., Yurtsever, Z., and Brett, T.J. (2015). Efficient Mammalian Cell Expression and Single-step Purification of Extracellular Glycoproteins for Crystallization. J. Vis. Exp. *23*, e53445.

Kolbe, E.W., Tamm, S., Hedtfeld, S., Becker, T., Tümmler, B., and Stanke, F. (2013). CLCA4 variants determine the manifestation of the cystic fibrosis basic defect in the intestine. Eur. J. Hum. Genet. *21*, 691–694.

Konarev, P.V., Volkov, V.V., Sokolova, A.V., Koch, M.H.J., and Svergun, D.I. (2003). PRIMUS: a Windows PC-based system for small-angle scattering data analysis. J. Appl. Cryst. *36*, 1277–1282.

Lacy, D.B., Wigelsworth, D.J., Melnyk, R.A., Harrison, S.C., and Collier, R.J. (2004a). Structure of heptameric protective antigen bound to an anthrax toxin receptor: a role for receptor in pH-dependent pore formation. Proc. Natl. Acad. Sci. USA *101*, 13147–13151.

Lacy, D.B., Wigelsworth, D.J., Scobie, H.M., Young, J.A., and Collier, R.J. (2004b). Crystal structure of the von Willebrand factor A domain of human capillary morphogenesis protein 2: an anthrax toxin receptor. Proc. Natl. Acad. Sci. USA *101*, 6367–6372.

Laskowski, R.A., and Swindells, M.B. (2011). LigPlot+: multiple ligand-protein interaction diagrams for drug discovery. J. Chem. Inf. Model. *51*, 2778–2786.

Lee, J.O., Rieu, P., Arnaout, M.A., and Liddington, R. (1995). Crystal structure of the A domain from the alpha subunit of integrin CR3 (CD11b/CD18). Cell *80*, 631–638.

Li, R., Rieu, P., Griffith, D.L., Scott, D., and Arnaout, M.A. (1998). Two functional states of the CD11b A-domain: correlations with key features of two Mn2+-complexed crystal structures. J. Cell Biol. *143*, 1523–1534.

Li, H., Salomon, J.J., Sheppard, D.N., Mall, M.A., and Galietta, L.J. (2017). Bypassing CFTR dysfunction in cystic fibrosis with alternative pathways for anion transport. Curr. Opin. Pharmacol. *34*, 91–97.

Luo, B.H., Carman, C.V., and Springer, T.A. (2007). Structural basis of integrin regulation and signaling. Annu. Rev. Immunol. *25*, 619–647.

Mahalingam, B., Ajroud, K., Alonso, J.L., Anand, S., Adair, B.D., Horenstein, A.L., Malavasi, F., Xiong, J.P., and Arnaout, M.A. (2011). Stable coordination of the inhibitory Ca2+ ion at the metal ion-dependent adhesion site in integrin CD11b/CD18 by an antibody-derived ligand aspartate: implications for integrin regulation and structure-based drug design. J. Immunol. *187*, 6393–6401.

Mall, M.A., and Galietta, L.J. (2015). Targeting ion channels in cystic fibrosis. J. Cyst. Fibros. *14*, 561–570.

Mall, M.A., Danahay, H., and Boucher, R.C. (2018). Emerging Concepts and Therapies for Mucoobstructive Lung Disease. Ann. Am. Thorac. Soc. *15*, S216–S226.

McCleverty, C.J., and Liddington, R.C. (2003). Engineered allosteric mutants of the integrin alphaMbeta2 I domain: structural and functional studies. Biochem. J. *372*, 121–127.

Meyer, P.A., Socias, S., Key, J., Ransey, E., Tjon, E.C., Buschiazzo, A., Lei, M., Botka, C., Withrow, J., Neau, D., et al. (2016). Data publication with the structural biology data grid supports live analysis. Nat. Commun. *7*, 10882.

Morin, A., Eisenbraun, B., Key, J., Sanschagrin, P.C., Timony, M.A., Ottaviano, M., and Sliz, P. (2013). Cutting edge: Collaboration gets the most out of software. eLife *2*, e01456.

Mundhenk, L., Erickson, N.A., Klymiuk, N., and Gruber, A.D. (2018). Interspecies diversity of chloride channel regulators, calcium-activated 3 genes. PLoS One *13*, e0191512.

Nolte, M., Pepinsky, R.B., Venyaminov SYu, Koteliansky, V., Gotwals, P.J., and Karpusas, M. (1999). Crystal structure of the alpha1beta1 integrin I-domain: insights into integrin I-domain function. FEBS Lett. *452*, 379–385.

Patel, A.C., Brett, T.J., and Holtzman, M.J. (2009). The role of CLCA proteins in inflammatory airway disease. Annu. Rev. Physiol. *71*, 425–449.

Paulino, C., Kalienkova, V., Lam, A.K.M., Neldner, Y., and Dutzler, R. (2017). Activation mechanism of the calcium-activated chloride channel TMEM16A revealed by cryo-EM. Nature *552*, 421–425.

Paulsson, M., and Wagener, R. (2018). Matrilins. Methods Cell Biol. *143*, 429–446.

Rambo, R.P. (2015). Resolving Individual Components in Protein-RNA Complexes Using Small-Angle X-ray Scattering Experiments. Methods Enzymol. *558*, 363–390.

Robert, X., and Gouet, P. (2014a). Deciphering key features in protein structures with the new ENDscript server. Nucleic Acids Res. *42*, W320–W324.

Romani, L., Oikonomou, V., Moretti, S., Iannitti, R.G., D'Adamo, M.C., Villella, V.R., Pariano, M., Sforna, L., Borghi, M., Bellet, M.M., et al. (2017). Thymosin α1 represents a potential potent single-molecule-based therapy for cystic fibrosis. Nat. Med. *23*, 590–600.

Rossmann, M.G., Moras, D., and Olsen, K.W. (1974). Chemical and biological evolution of nucleotide-binding protein. Nature *250*, 194–199.

Ruffin, M., Voland, M., Marie, S., Bonora, M., Blanchard, E., Blouquit-Laye, S., Naline, E., Puyo, P., Le Rouzic, P., Guillot, L., et al. (2013). Anoctamin 1 dysregulation alters bronchial epithelial repair in cystic fibrosis. Biochim. Biophys. Acta *1832*, 2340–2351.

Sala-Rabanal, M., Yurtsever, Z., Berry, K.N., and Brett, T.J. (2015a). Novel Roles for Chloride Channels, Exchangers, and Regulators in Chronic Inflammatory Airway Diseases. Mediators Inflamm. *2015*, 497387.

Sala-Rabanal, M., Yurtsever, Z., Nichols, C.G., and Brett, T.J. (2015b). Secreted CLCA1 modulates TMEM16A to activate Ca(2+)-dependent chloride currents in human cells. eLife *4*, e05875.

Sala-Rabanal, M., Yurtsever, Z., Berry, K.N., Nichols, C.G., and Brett, T.J. (2017). Modulation of TMEM16A channel activity by the von Willebrand factor type A (VWA) domain of the calcium-activated chloride channel regulator 1 (CLCA1). J. Biol. Chem. *292*, 9164–9174.

San Sebastian, E., Mercero, J.M., Stote, R.H., Dejaegere, A., Cossío, F.P., and Lopez, X. (2006). On the affinity regulation of the metal-ion-dependent adhesion sites in integrins. J. Am. Chem. Soc. *128*, 3554–3563.

Santelli, E., Bankston, L.A., Leppla, S.H., and Liddington, R.C. (2004). Crystal structure of a complex between anthrax toxin and its host cell receptor. Nature *430*, 905–908.

Shimaoka, M., Takagi, J., and Springer, T.A. (2002). Conformational regulation of integrin structure and function. Annu. Rev. Biophys. Biomol. Struct. *31*, 485–516.

Shimaoka, M., Xiao, T., Liu, J.H., Yang, Y., Dong, Y., Jun, C.D., McCormack, A., Zhang, R., Joachimiak, A., Takagi, J., et al. (2003). Structures of the alpha L I domain and its complex with ICAM-1 reveal a shape-shifting pathway for integrin regulation. Cell *112*, 99–111.

Sievers, F., Wilm, A., Dineen, D., Gibson, T.J., Karplus, K., Li, W., Lopez, R., McWilliam, H., Remmert, M., Söding, J., et al. (2011). Fast, scalable generation of high-quality protein multiple sequence alignments using Clustal Omega. Mol. Syst. Biol. *7*, 539.

Sondo, E., Caci, E., and Galietta, L.J. (2014). The TMEM16A chloride channel as an alternative therapeutic target in cystic fibrosis. Int. J. Biochem. Cell Biol. *52*, 73–76.

Song, G., and Springer, T.A. (2014). Structures of the Toxoplasma gliding motility adhesin. Proc. Natl. Acad. Sci. USA *111*, 4862–4867.

Song, G., Koksal, A.C., Lu, C., and Springer, T.A. (2012). Shape change in the receptor for gliding motility in *Plasmodium* sporozoites. Proc. Natl. Acad. Sci. USA *109*, 21420–21425.

Sonneville, F., Ruffin, M., Coraux, C., Rousselet, N., Le Rouzic, P., Blouquit-Laye, S., Corvol, H., and Tabary, O. (2017). MicroRNA-9 downregulates the

ANO1 chloride channel and contributes to cystic fibrosis lung pathology. Nat. Commun. *8*, 710.

Springer, T.A. (2006). Complement and the multifaceted functions of VWA and integrin I domains. Structure *14*, 1611–1616.

Svergun, D.I. (1992). Determination of the Regularization Parameter in Indirect-Transform Methods Using Perceptual Criteria. J. Appl. Cryst. *25*, 495–503.

van der Doef, H.P., Slieker, M.G., Staab, D., Alizadeh, B.Z., Seia, M., Colombo, C., van der Ent, C.K., Nickel, R., Witt, H., and Houwen, R.H. (2010). Association of the CLCA1 p.S357N variant with meconium ileus in European patients with cystic fibrosis. J. Pediatr. Gastroenterol. Nutr. *50*, 347–349.

Veit, G., Bossard, F., Goepp, J., Verkman, A.S., Galietta, L.J., Hanrahan, J.W., and Lukacs, G.L. (2012). Proinflammatory cytokine secretion is suppressed by TMEM16A or CFTR channel activity in human cystic fibrosis bronchial epithelia. Mol. Biol. Cell *23*, 4188–4202.

Volkov, V.V., and Svergun, D.I. (2003). Uniqueness of ab initio shape determination in small-angle scattering. J. Appl. Cryst. *36*, 860–864.

Vorup-Jensen, T., Ostermeier, C., Shimaoka, M., Hommel, U., and Springer, T.A. (2003). Structure and allosteric regulation of the alpha X beta 2 integrin I domain. Proc. Natl. Acad. Sci. USA *100*, 1873–1878.

Vorup-Jensen, T., Waldron, T.T., Astrof, N., Shimaoka, M., and Springer, T.A. (2007). The connection between metal ion affinity and ligand affinity in integrin I domains. Biochim. Biophys. Acta *1774*, 1148–1155.

Whittaker, C.A., and Hynes, R.O. (2002). Distribution and evolution of von Willebrand/integrin A domains: widely dispersed domains with roles in cell adhesion and elsewhere. Mol. Biol. Cell *13*, 3369–3387.

Wriggers, W., and Chacon, P. (2001). Using Situs for the registration of protein structures with low-resolution bead models from X-ray solution scattering. J. Appl. Cryst. *34*, 773–776.

Wu, J., Yan, Z., Li, Z., Yan, C., Lu, S., Dong, M., and Yan, N. (2015). Structure of the voltage-gated calcium channel Cav1.1 complex. Science *350*, aad2395.

Wu, J., Yan, Z., Li, Z., Qian, X., Lu, S., Dong, M., Zhou, Q., and Yan, N. (2016). Structure of the voltage-gated calcium channel Ca(v)1.1 at 3.6 Å resolution. Nature *537*, 191–196.

Young, F.D., Newbigging, S., Choi, C., Keet, M., Kent, G., and Rozmahel, R.F. (2007). Amelioration of cystic fibrosis intestinal mucous disease in mice by restoration of mCLCA3. Gastroenterology *133*, 1928–1937.

Yurtsever, Z., Sala-Rabanal, M., Randolph, D.T., Scheaffer, S.M., Roswit, W.T., Alevy, Y.G., Patel, A.C., Heier, R.F., Romero, A.G., Nichols, C.G., et al. (2012). Self-cleavage of human CLCA1 protein by a novel internal metalloprotease domain controls calcium-activated chloride channel activation. J. Biol. Chem. *287*, 42138–42149.

Zhang, Q., Zhou, Y.F., Zhang, C.Z., Zhang, X., Lu, C., and Springer, T.A. (2009). Structural specializations of A2, a force-sensing domain in the ultralarge vascular protein von Willebrand factor. Proc. Natl. Acad. Sci. USA *106*, 9226–9231.

STAR★METHODS

KEY RESOURCES TABLE

REAGENT or RESOURCE	SOURCE	IDENTIFIER
Antibodies		
HRP Conjugated Anti-6-histidine	Bethyl Laboratories	Cat# A190-114P; RRID: AB_162722
Deposited Data		
Raw and Analyzed Data CLCA1 VWA 302-476	This paper	PDB: 6PYO
Raw and Analyzed Data CLCA1 VWA 302-478	This paper	PDB: 6PYX
CLCA1 VWA 302-476 Coordinates	This paper	PDB: 6PYO
CLCA1 VWA 302-478 Coordinates	This paper	PDB: 6PYX
CLCA1 VWA 302-476 SAXS	This paper	SASBDB: SASDH24
CLCA1 CAT-CYS-VWA 22-477 SAXS	This paper	SASBDB: SASHD34
Experimental Models: Cell Lines		
Expi293F	ThermoFisher	Cat# A14527; RRID: CVCL_D615
HEK293T	ATCC	Cat# CRL-3216; RRID: CVCL_0063
Oligonucleotides		
Primers for CLCA1 constructs and mutants, see Table S1	This paper	N/A
Recombinant DNA		
pHLsec	(Aricescu et al., 2006)	N/A
pcDNA 3.1	ThermoFisher	Cat# V79020
Software and Algorithms		
Chirascan Software	Applied Photophysics	https://www.photophysics.com/systems/chirascan-systems/chirascan/system-information/
Protein Thermal Shift Software	ThermoFisher	Cat#4466038
PHENIX	(Adams et al., 2010)	http://www.phenix-online.org/
COOT	(Emsley et al., 2010)	https://www2.mrc-lmb.cam.ac.uk/personal/pemsley/coot/
PyMOL	Schrodinger, LLC	https://www.schrodinger.com/
XDS	(Kabsch, 2010)	http://xds.mpimf-heidelberg.mpg.de/
ATSAS	(Franke et al., 2017)	https://www.embl-hamburg.de/biosaxs/software.html

LEAD CONTACT AND MATERIALS AVAILABILITY

Further information and requests for resources and reagents should be directed to and will be fulfilled by the Lead Contact, Tom J. Brett (tbrett@wustl.edu). All unique/stable reagents generated in this study are available from the Lead Contact without restriction.

EXPERIMENTAL MODEL AND SUBJECT DETAILS

Cell Lines

Expi293F cells (RRID: CVCL_D615; sex = female) used for high-level protein expression were cultured at 37°C and 8% CO_2 in serum-free Expi293 Expression Media (ThermoFisher Scientific) supplemented with 0.5% penicillin/streptomycin (Pen/Strep, GIBCO). Human embryonic kidney 293T cells (ATCC Cat # CRL-3216, RRID: CVCL_0063; sex = female) were cultured at 37°C and 5% CO_2 in Dulbecco's modified Eagle's medium (GIBCO) supplemented with 10% Fetal Bovine Serum (FBS), 1% Non-essential Amino Acids (Corning Inc., Corning, NY), 1% Glutamax (GIBCO) and 1% penicillin/streptomycin (Pen/Strep, GIBCO).

METHOD DETAILS

Expression constructs

Human CLCA1 VWA domain constructs (302-476 and 302-478) and CAT-CYS-VWA (22-477) were cloned into the mammalian cell expression vector pHLsec, which contains an optimized signal sequence and C-terminal 6-histidine tag for purification (Aricescu

et al., 2006). Mutants (C308S, C386S, C421S and C386S/C421S) were first generated in full-length CLCA1 in the vector pcDNA 3.1 using QuikChange Lightning Site-Directed Mutagenesis Kit (Agilent, Santa Clara, CA) (primer sequences in Table S1) and then subcloned into pHLsec. All constructs were verified by sequencing.

Protein expression and purification

WT human CLCA1 VWA domains (302-476 and 302-478) and CAT-CYS-VWA (22-477) were expressed in Expi293 cells via transient transfection with either Hype-5 or Hype-293 (OZ Biosciences, San Diego, CA) at a 1:1.5 ratio (μg of DNA: μL of transfection reagent) using 1 μg of plasmid per 1 million cells, similar to our previous reports (Kober et al., 2015). Media from supernatants were harvested after 72-96 hours by centrifugation, concentrated to 1/10 of the original volume using a 10 kDa cutoff membrane (Ultracel Ultrafiltration Discs, EMD Millipore) and adjusted to pH 8.5 and 5 mM imidazole. The concentrated protein was purified using Ni-NTA Superflow resin (QIAGEN, Hilden, Germany) and eluted in 5 mL of buffer containing 50 mM K_2HPO_4 (pH 8), 300 mM NaCl, and 250 mM imidazole. The eluted protein was concentrated and purified by size exclusion chromatography (Superdex75 Increase 10/300 GL for VWA in 20 mM Tris (pH 8) and 150 mM NaCl and Superdex 200 Increase 10/300 GL for CAT-CYS-VWA in 20 mM HEPES and 150 mM NaCl (pH 7.4), GE Healthcare). Purified CLCA1 VWA was dialyzed into buffer containing 20 mM HEPES (pH 7.4) and 150 mM NaCl and concentrated in a 10,000 kDA cutoff centrifuge concentrator (Vivaspin 500, Sartorius) to 12 mg ml^{-1}, as calculated from absorbance at 280 nm, for crystallization. Protein purity was assessed by Coomassie staining of SDS-PAGE.

Crystallization, structure determination, and analysis

Crystals of CLCA1 VWA (302-476) were grown at 17°C by hanging drop vapor diffusion by mixing 1:1 with well solution containing 0.2 M HEPES pH 7.5, 0.1 M $CaCl_2$, 28% PEG 400 or by streak seeding into the same conditions containing 5% glycerol. Crystals formed within 6 days. Crystals were flash frozen under a nitrogen stream at −160°C. Data were collected at the Advanced Light Source, beamline 4.2.2 (Berkeley, CA) and scaled and processed to 2.0 Å using XDS (Kabsch, 2010). A molecular replacement solution was found with PHASER (TFZ = 10.2) using uncharacterized membrane spanning protein from *Vibrio fischeri* (4RCK) (poly-Ala model) as the probe, locating two molecules in the asymmetric unit (ASU) for a solvent content of 61%. The initial solution was refined by rigid body refinement in PHENIX (Adams et al., 2010) and initially built using AUTOBUILD in PHENIX. The model was improved by iterative rounds of manual rebuilding in COOT (Emsley et al., 2010) and refinement using PHENIX. Secondary structure restraints were used during refinement and hydrogens were added as a riding model in the final rounds. Simulated annealing was used early in refinement, and optimization of X-ray and ADP or stereochemistry weight was applied in later rounds. The final model is 94% complete with 17 C-terminal residues (460-476) in both chains and the first N- terminal residue (302) in chain B not visible in the electron density. Chain A contained three N-terminal residues (ETG 299-301) that are a remnant of the vector-encoded signal sequence (Aricescu et al., 2006). LigPlot+ (Laskowski and Swindells, 2011) was used to analyze cation contacts. Solvent accessibility calculations were carried out using NACCESS (Hubbard and Thornton, 1993). For structure-based alignment, amino acid sequences were aligned using Clustal Omega (Sievers et al., 2011) and residue conservation scored by ESPript (Robert and Gouet, 2014a). Secondary structure predictions were generated in JPRED4 (Drozdetskiy et al., 2015). All crystallographic and analysis software used were compiled and distributed by the SBGrid resource (Morin et al., 2013) and diffraction images were archived with the SB Data Grid (Meyer et al., 2016). Crystals of CLCA1 VWA (302-478) were grown under similar conditions and diffracted to 2.6 Å. The structure was solved by isostructural replacement of CLCA1 VWA (302-476), and iteratively refined and rebuilt as above. The final model consisted of residues 302-461 (chain A) and 303-459 (chain B).

Small angle X-ray scattering

SAXS data was obtained at the Advanced Light Source on the SIBYLS beamline 12.3.1 (Dyer et al., 2014). Thirty-three exposures of 0.3 s were obtained for each protein at 1-10 mg/mL and scattering from the dialysis buffer (20 mM HEPES pH 7.4, 150 mM NaCl, and 2% glycerol) was subtracted. Data were inspected for quality and scale-merged in scÅtter 3.0g (Rambo, 2015). Data was subsequently analyzed in the ATSAS 2.8.4 suite (Franke et al., 2017) using PRIMUS (Konarev et al., 2003). Guinier analysis showed no radiation damage, aggregation or concentration effects. I(0) and the pair distance distribution function P(r) were calculated in GNOM (Svergun, 1992) within PRIMUS. Ten low-resolution *ab initio* models from DAMMIN (Franke and Svergun, 2009) were automatically averaged using DAMAVER (Volkov and Svergun, 2003) and converted to a surface map using SITUS (Wriggers and Chacon, 2001).

Graphical Representation of Structures

All molecular graphics images were produced using PyMOL.

Heterologous expression of CLCA1 and Western Blotting

HEK293T cells were grown to 70%–90% confluency and transfected with CLCA1 VWA domain constructs and 293Fectin at a 1:2 ratio (μg of DNA: μL of transfection reagent) using 1 μg of plasmid DNA per 1 million cells. After 24 hours, supernatants were mixed with 2x SDS containing 2-mercaptoethanol sample buffer. Cells were pelleted and lysed in PBS-1% Triton X-100, then diluted in 2x SDS containing 2-mercaptoethanol sample buffer and sonicated. Samples were boiled for 5 minutes, then loaded on a 4%–12% Bis-Tris NuPage gel (Life Technologies). Proteins were transferred to nitrocellulose membranes using an iBlot Gel transfer device (Life Technologies). Membranes were blocked with 0.5% blotting-grade blocker nonfat milk (Bio-Rad) in PBS with 0.1% Tween-20. HRP-conjugated anti-6-histidine antibody (Bethyl Laboratories) diluted 1:5000 in blocking buffer was incubated on the

membrane for 10 minutes at room temperature. Following three washes with PBS-Tween-20, signal was detected using Pierce ECL Western Blotting Substrate (Thermo Fisher Scientific, Rockford, IL). Developed films were scanned.

Circular Dichroism

CD spectroscopy measurements were performed using an Chirascan spectropolarimeter equipped with a Peltier temperature controller (Applied Photophysics). A 1 cm path length cuvette was used and the protein concentration was 50 μg/mL. Thermal denaturation experiments were carried out in 20 mM Tris pH 8.0, 100 mM NaCl and 1 mM of either EDTA, $MgCl_2$, or $CaCl_2$. For reducing conditions, the buffer contained 1 mM DTT. Ellipticity was measured at 222 nm in 1°C steps from 20 to 90°C at a rate of 1°C/min. Data was analyzed using ProScan software (Applied Photophysics).

Differential Scanning Fluorimetry

Thermal stability was assessed by differential scanning fluorimetry (DSF) on protein purified by size exclusion chromatography. The Protein Thermal Shift kit (Applied Biosystems) was used according to manufacturer's instructions. Briefly, protein was concentrated to 0.5 mg/mL after buffer exchange into 20 mM HEPES pH 7.5, 150 mM NaCl and 1 mM of either EDTA, $MgCl_2$, $CaCl_2$ or DTT. 5 μL of reaction buffer and 2.5 μL 8x fluorescent dye were added to 12.5 μL protein on ice. Melt-curve experiments were performed using Fast7500 qPCR machine (Applied Biosystems) starting at 25°C and with continuous 1% ramp to 95°C (roughly at 1°C/min). The data were analyzed using Protein Thermal Shift software (Applied Biosystems).

QUANTIFICATION AND STATISTICAL ANALYSIS

Statistical analyses for differential scanning fluorimetry (DSF) experiments, specifically for melting temperature (T_M) determination, were performed using Protein Thermal Shift software (Applied Biosystems). Representative derivative-curve melting temperatures from three (n = 3) independent experiments are shown. Melting temperature data are represented as mean ± SEM of triplicate (n = 3) samples. For circular dichroism (CD) experiments, statistical analyses, specifically for T_M determination, were performed using the ProScan software (Applied Photophysics). Representative spectra of three (n = 3) independent experiments is shown. CD spectra are plotted as mean ellipticity per residue ± SD of triplicate (n = 3) recordings. Melting temperature data are represented as the calculated melting temperature using a sigmoid curve fit and estimated error reported from the ProScan software. Statistical details are also included in Figure 3 legends.

DATA AND CODE AVAILABILITY

Coordinates and structure factors for CLCA1 VWA (302-476) and CLCA1 VWA (302-478) have been deposited in the RCSB Protein Data Bank with accession numbers PBD: 6PYO and 6PYX, respectively. SAXS data for CLCA1 VWA (302-476) and CLCA1 CAT-CYS-VWA (22-477) have been deposited in the SASBDB with accession numbers SASBDB: SASDH24 and SASDH34, respectively.

Cell Reports, Volume *30*

Supplemental Information

Structural and Biophysical Analysis of the CLCA1 VWA Domain Suggests Mode of TMEM16A Engagement

Kayla N. Berry and Tom J. Brett

Related to Methods

Table S1. Primer sequences used in study	
Primer	**5' – 3' sequence**
hCLCA1 VWA (302-476) forward	GAAACCGGTATTGGACAAAGAATTGTGTGT
hCLCA1 VWA (302-476) reverse	CGGGGTACCTGAAAGGGCCCCAAAAGCATC
hCLCA1 VWA (302-478) forward	GAAACCGGTATTGGACAAAGAATTGTGTGT
hCLCA1 VWA (302-478) reverse	CGGGGTACCTCCTGATGAAAGGGCCCCAAAAGC
hCLCA1 CAT-CYS-VWA (22-477) forward	GAAACCGGTAATTCACTCATTCAGCTGAAC
hCLCA1 CAT-CYS-VWA (22-477) reverse	CGGGGTACCTGAAAGGGCCCCAAAAGCATC
hCLCA1 C308S forward	GGTATTGGACAAAGAATTGTGAGTTTAGTCCTTGACAAATCTG
hCLCA1 C308S reverse	CAGATTTGTCAAGGACTAAACTCACAATTCTTTGTCCAATACC
hCLCA1 C386S forward	GGGACGTCCATCAGCAGCGGGCTTC
hCLCA1 C386S reverse	GAAGCCCGCTGCTGATGGACGTCCC
hCLCA1 C421S forward	GACAACACTATAAGTGGGAGCTTTAACGAGGTCAAAC
hCLCA1 C421S reverse	GTTTGACCTCGTTAAAGCTCCCACTTATAGTGTTGTC
hCLCA1 E157Q forward	AGGGCATTTGTCCATCAGTGGGCTCATCTA
hCLCA1 E157Q reverse	ACCTTGTGGTCCATATTCAGCTAACTTTTT

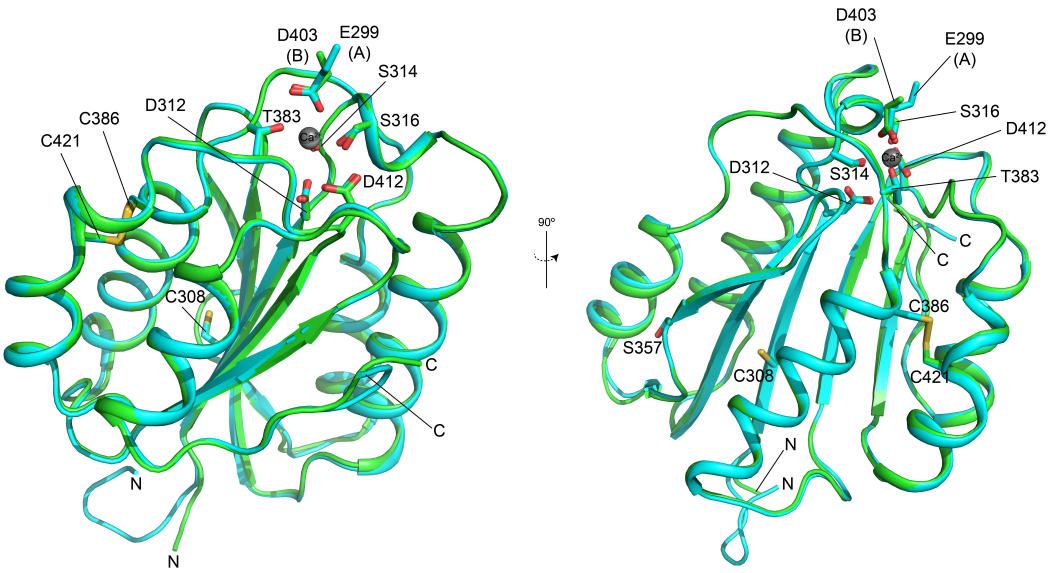

Figure S1 (Related to Figure 1). Superposition of hCLCA1 VWA Domain Chains A and B within the Asymmetric Unit

A) Alignment of hCLCA1 VWA domain chains A (cyan) and B (green) within the asymmetric unit, with a C_α RMSD of 0.3 Å. MIDAS residues, invariant disulfides and S357 are highlighted. Pseudoligand residue from chain A (E299) and chain B (D403) are also shown. The N-termini (N) and C-termini (C) of each chain are labeled.

Related to Table 1

Table S2. Crystallographic statistics for human CLCA1 VWA 302-478	
Data collection statistics	
Space Group	C2
Unit Cell	
a, b, c (Å)	103.4, 74.5, 75.4
α, β, γ (º)	90, 109.4, 90
Source	ALS 4.2.2
Wavelength(Å)	1.0000
Resolution(Å)	59.79 – 2.60 (2.72-2.60)
R_{merge}	0.266 (1.734)
$CC_{1/2}$	0.977 (0.328)
Completeness(%)	99.6 (98.1)
Redundancy	3.6 (3.3)
I/σ(I)	4.6 (0.6)
Refinement statistics	
R_{work} (%)	21.82
R_{free} (%)	27.87
Amino Acid Residues(#)	320
Waters (#)	82
RMSD bond length (Å)/angles(°)	0.008/0.906
Wilson B ($Å^2$)	40.5
Average B protein ($Å^2$)	42.32
Average B water ($Å^2$)	40.62
Average B Ca^{2+} ($Å^2$)	40.12
Ramachandran	
%Favored	94.3
%Allowed	5.7
%Outliers	0
Rotamer outliers (%)	0
Clashscore	8.91
Molprobity	1.86
Luzzati Error	0.393
PDB ID	6PYX

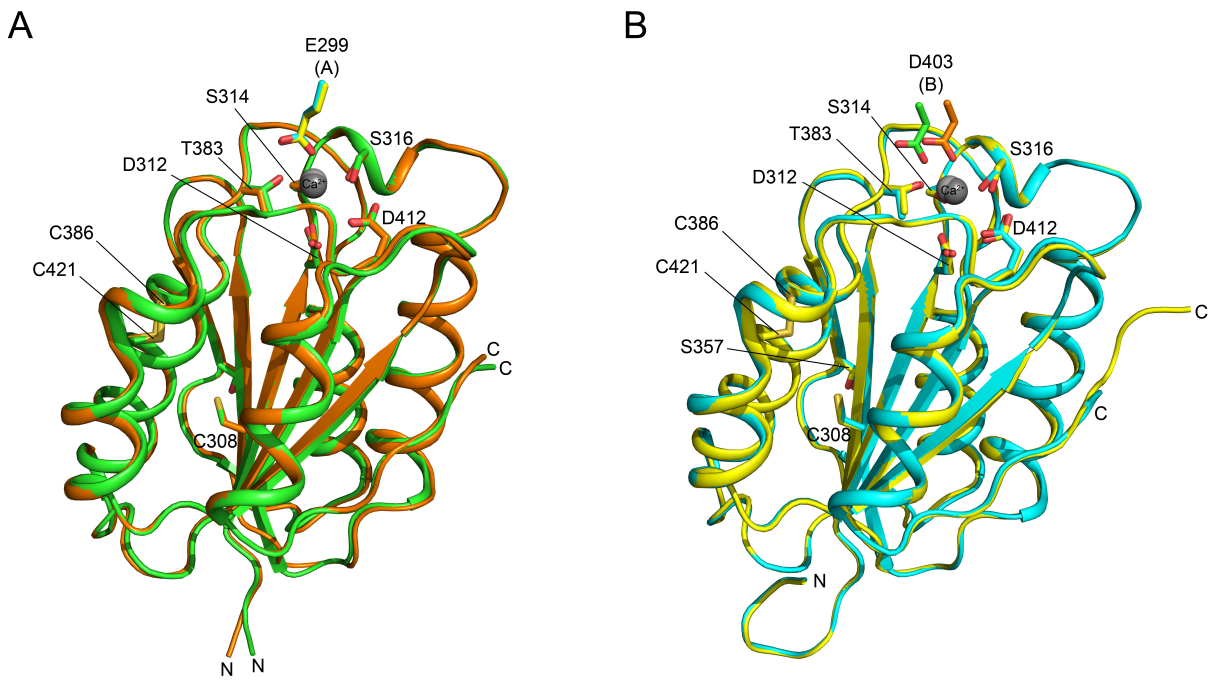

Figure S2 (Related to Figure 1). Superposition of crystal structures of CLCA1 VWA Domain 302-476 and 302-478. The structures are extremely similar (Cα RMSD of 0.33 Å). A) Alignment of chain B from CLCA1 VWA domain constructs containing residues 302-476 (green) and residues 302-478 (orange). B) Alignment of chain A from hCLCA1 VWA domain constructs containing residues 302-476 (cyan) and residues 302-478 (yellow). MIDAS residues, invariant disulfides and S357 are highlighted. Pseudo-ligand residue from chain A (E299) and chain B (D403) are also shown. The N-termini (N) and C-termini (C) of each chain are labeled.

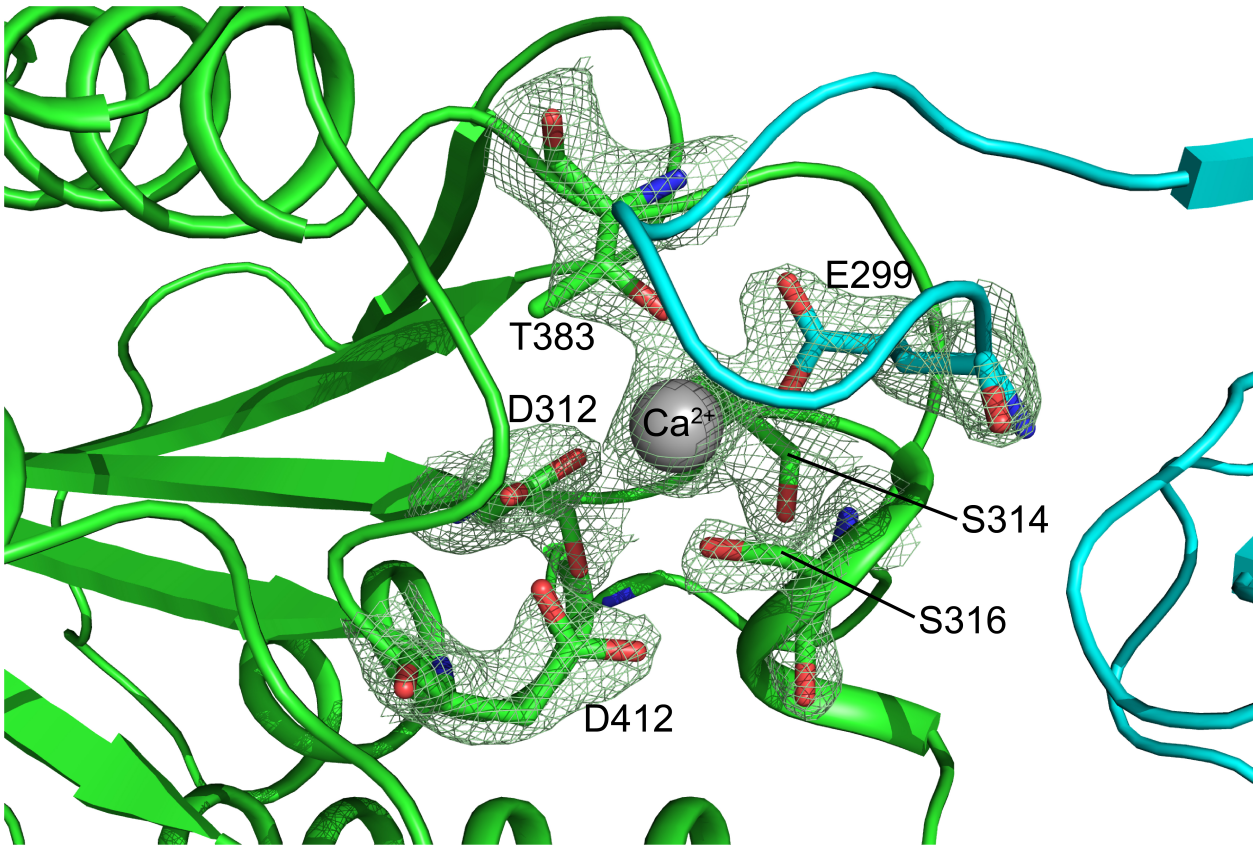

Figure S3 (Related to Figure 2). Difference Electron Density for the MIDAS and Ca^{2+} Ion

Difference electron density (2mFo-DFc contoured at 2σ) for the CLCA1 VWA MIDAS residues of chain B (green), including E299 from chain A (cyan) and calcium ion (grey).